LETTER

doi:10.1038/nature09776

A terahertz metamaterial with unnaturally high refractive index

Muhan Choi[1]†*, Seung Hoon Lee[1]*, Yushin Kim[1], Seung Beom Kang[2], Jonghwa Shin[3], Min Hwan Kwak[2], Kwang-Young Kang[2], Yong-Hee Lee[3], Namkyoo Park[4] & Bumki Min[1]

Controlling the electromagnetic properties of materials, going beyond the limit that is attainable with naturally existing substances, has become a reality with the advent of metamaterials[1–3]. The range of various structured artificial 'atoms' has promised a vast variety of otherwise unexpected physical phenomena[3–17], among which the experimental realization of a negative refractive index has been one of the main foci thus far. Expanding the refractive index into a high positive regime will complete the spectrum of achievable refractive index and provide more design flexibility for transformation optics[9–14]. Naturally existing transparent materials possess small positive indices of refraction, except for a few semiconductors and insulators, such as lead sulphide or strontium titanate, that exhibit a rather high peak refractive index at mid- and far-infrared frequencies[18]. Previous approaches using metamaterials were not successful in realizing broadband high refractive indices[19–21]. A broadband high-refractive-index metamaterial structure was theoretically investigated only recently[22], but the proposed structure does not lend itself to easy implementation. Here we demonstrate that a broadband, extremely high index of refraction can be realized from large-area, free-standing, flexible terahertz metamaterials composed of strongly coupled unit cells. By drastically increasing the effective permittivity through strong capacitive coupling and decreasing the diamagnetic response with a thin metallic structure in the unit cell, a peak refractive index of 38.6 along with a low-frequency quasi-static value of over 20 were experimentally realized for a single-layer terahertz metamaterial, while maintaining low losses. As a natural extension of these single-layer metamaterials, we fabricated quasi-three-dimensional high-refractive-index metamaterials, and obtained a maximum bulk refractive index of 33.2 along with a value of around 8 at the quasi-static limit.

According to the Maxwellian macroscopic description, the effective relative permittivity of an artificial medium can be written as $\varepsilon = 1 + (P/\varepsilon_0 E)$ and the effective relative permeability can be defined by $\mu = 1 + (M/H)$, where E, H, P and M denote electric field, magnetizing field, polarization and magnetization, respectively. In order to tailor the value of the refractive index by controlling the degree of polarization and magnetization, we used a strongly coupled, thin 'I'-shaped metallic patch to maximize the effective permittivity ε while suppressing the diamagnetic effect. A similar 'I'-shaped patch structure in the weakly and moderately coupled regimes has been used to provide the index variations required for broadband ground-plane cloaking in the microwave frequency bands[12].

The basic building block (single-layer unit cell) of the proposed high-refractive-index terahertz metamaterial is shown in Fig. 1a, together with the polarization of an incident terahertz wave. (In Supplementary Information we describe the polarization dependence of this system. We note that two-dimensionally isotropic high-index metamaterials can be designed; the results are given in Supplementary Information.) Here, the substrate is made from a dielectric material and the thin 'I'-shaped metallic patch is embedded symmetrically in the substrate. Throughout this work, the substrate was implemented with polyimide (real part of the refractive index n, Re(n), is 1.8) and the metals used to construct the metamaterials were gold (on chromium) or aluminium (see Methods Summary). Optical micrographs of the fabricated large-area (2 × 2 cm), free-standing, flexible metamaterials are shown in Fig. 1b. Precise alignment between stacked metamaterial layers has been achieved, as can be confirmed by the higher-magnification microscope images shown in the upper insets of Fig. 1b. As the substrate is made from flexible polyimide, the fabricated metamaterials are also extremely flexible, and the samples are perfectly free-standing (lower inset of Fig. 1b).

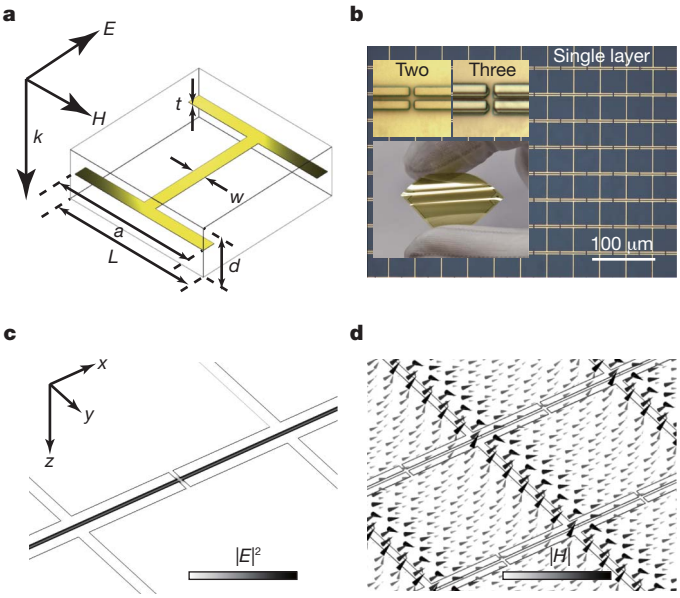

Figure 1 | Schematic view of the high-index metamaterials and images of the fabricated metamaterials. **a**, Unit cell structure of the high-index metamaterial, made of a thin 'I'-shaped metallic patch symmetrically embedded in a dielectric material. The incident terahertz wave is directed downwards, with the polarization of the wave indicated by the arrows. **b**, Optical micrograph of fabricated single-layer metamaterial. Top insets, higher-magnification micrographs, showing the alignment of constituent metamaterial layers for double- and triple-layer metamaterials. Bottom inset, photograph of a flexibility test for the fabricated metamaterials. **c**, Saturated electric field (at 0.33 THz) for a single-layer metamaterial with a unit cell of $L = 60$ μm, $a = 58.8$ μm, $d = 2.45$ μm, and $w = 3$ μm. Shading indicates modulus of field to the power two. **d**, Vector plot of the magnetic field (at 0.33 THz) in the unit cells. Shading indicates modulus of field.

[1]Department of Mechanical Engineering, Korea Advanced Institute of Science and Technology (KAIST), Daejeon 305-751, South Korea. [2]Convergence Components and Materials Research Laboratory, Electronics and Telecommunications Research Institute (ETRI), Daejeon 305-700, South Korea. [3]Department of Physics, Korea Advanced Institute of Science and Technology (KAIST), Daejeon 305-751, South Korea. [4]School of Electrical Engineering and Computer Science, Seoul National University, Seoul 151-744, South Korea. †Present address: Convergence Components and Materials Research Laboratory, Electronics and Telecommunications Research Institute (ETRI), Daejeon 305-700, South Korea.
*These authors contributed equally to this work.

The gap width (defined by $g = L - a$; see Fig. 1a for details) plays a crucial role in raising the effective permittivity. For the thin 'I'-shaped metallic patch structure, the scaling of the charge accumulation and effective permittivity shows different asymptotic behaviours depending on the gap width, leading to weakly coupled ($g/L \lesssim 1$) and strongly coupled ($g/L \ll 1$) regimes. In the strongly coupled regime, a large amount of surface charge is accumulated on each arm of the metallic patch capacitor as the charges in each arm interact with opposite charges in close proximity across the gap. Charge accumulation on the edge of the metallic patch leads to an extremely large dipole moment in the unit cell, as the accumulated charge is inversely proportional to the gap width in the strongly coupled regime ($Q \propto L^3 g^{-1}$). This extreme charge accumulation contributes to a huge dipole moment inside the unit cell (or a large polarization density) and ultimately leads to a large effective permittivity. The behaviour of the charge accumulation differs significantly in the weakly coupled regime, in which the amount of charge increases quadratically with decreasing gap width ($Q \propto (L - g)^2$) in the quasi-static limit (Supplementary Information).

Although decreasing the gap width can enhance the effective permittivity, it is still necessary to suppress the diamagnetic effect to realize a high refractive index. A thin 'I'-shaped metallic structure can provide a pathway to effectively reduce the diamagnetic effect, as a thin 'I'-shaped patch has a small area subtended by the current loops[22] (Supplementary Information). To put this theoretical argument into practice, all the metamaterial samples used in this work featured thin metallic structures, the thicknesses of which were of the order of a skin depth (less than 100 nm) in the terahertz frequency range. To confirm the physical origin of the high refractive index with the aforementioned approach, the electric and magnetic field around the metallic patch in the unit cells of a single-layer metamaterial were calculated for a frequency of 0.33 THz (Fig. 1c, d). As described above, the electric field was strongly concentrated in the gap and the magnetic field penetrated deeply into the unit cell because of the negligible metallic volume fraction (Supplementary Information).

In order to quantify the effect of extremely large dipole moments and weak diamagnetism associated with the proposed metamaterials, an effective parameter retrieving method was used to extract relevant material parameters, such as refractive index n and impedance z (or equivalently, the effective permittivity $\varepsilon = nz_0/z$ and the permeability $\mu = nz/z_0$, where z_0 is the impedance of free space) from the scattering parameters[23] (S parameters). As can be confirmed from Fig. 2a, a strong electrical resonance was observed with a peak relative permittivity of 583 at a frequency of 0.504 THz and of 122 at the quasi-static limit; these values are remarkably higher than those of bare polyimide films[24] ($\mathrm{Re}(\varepsilon) \approx 3.24$). The magnetic permeability, however, remained near unity over the whole frequency domain, except near the frequency of the electric resonance, where a weak magnetic anti-resonance accompanying the strong electrical resonance was observed[25]. By virtue of this extreme enhancement of permittivity along with the suppression of diamagnetism, a peak index of refraction of $n = 27.25$ at 0.516 THz was predicted, along with a value of $n = 11.1$ at the quasi-static limit. This unprecedented 'amplification' of refractive index relative to that of a host dielectric material shows the efficacy of employing strongly polarizable and weakly diamagnetic metallic patches. Considering the effective wavelength of a terahertz wave inside the metamaterial, the thickness ($d = 2.45$ μm) in the direction of propagation is much smaller than the effective wavelength ($d \leq 0.12\lambda/n$), which justifies the application of homogenization theory[2,3] and the effective parameter descriptions. For the assignment of effective refractive indices to the single-layer metamaterial, we have used the physical thickness for consistent estimation of all effective parameters in the retrieval method. However, actual effective refractive index is slightly lower than the index acquired with physical thickness, as effective thickness should be introduced to account for the effect of mode decay in a single-layer metamaterial (Methods).

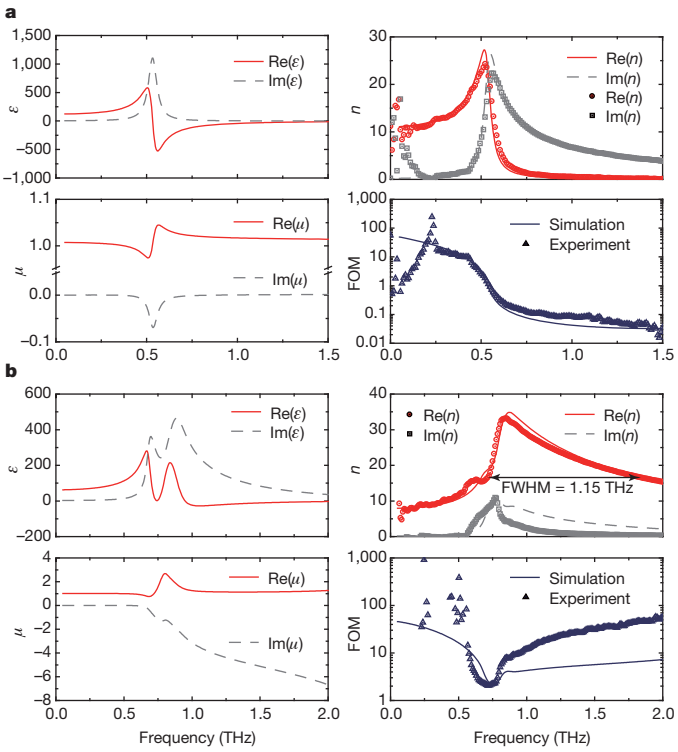

Figure 2 | Extracted effective permittivity, permeability, refractive index and figure of merit for high-index metamaterials. **a**, Effective permittivity (ε, top left) and permeability (μ, bottom left) extracted from the characterization of a single-layer metamaterial unit cell. Experimentally obtained complex refractive index (n) is shown top right, along with the corresponding numerically extracted values from the S-parameter retrieval method. Bottom right, the experimental figure of merit (FOM) together with the numerically obtained values. Geometrical parameters of the unit cell are the same as those used for the simulation performed for Fig. 1c and d. In the plots, data points and lines are used for the experimental and numerical data, respectively. **b**, As **a** but for a five-layer metamaterial. Here, the gap width g is set to 1.5 μm, the length of a unit cell L is 40 μm, the width of metallic structure w is 3 μm, and the thickness d of the unit cell is 1.62 μm with an additional polyimide layer of ~0.8 μm on both the top and bottom of the fabricated metamaterials.

To experimentally probe the enhancement of the effective refractive index, terahertz time-domain spectroscopy[26] (THz-TDS) was performed for a frequency range of 0.1–2 THz. All the samples were prepared with conventional micro/nano-fabrication processes (see Methods Summary). For reliable extraction of the complex refractive index from the THz-TDS experiments, an iterative algorithm considering multi-pass transmission through the sample was applied to the field transmission data (Methods)[27]. Next, the complex refractive indices extracted from the THz-TDS measurements were compared with the numerically obtained refractive indices from the S-parameter extraction methods (Fig. 2a). Considering the uncertainties in the material parameters used for the simulation and the errors in the gap-width measurements, the experimentally acquired complex refractive index was in excellent agreement with the simulated refractive index. From the characterization of the single-layer metamaterial, a peak refractive index of $n = 24.34$ at 0.522 THz was observed, with a value of $n = 11.18$ at the quasi-static limit. The loss associated with the single-layer metamaterial is quantified by the figure of merit ($\mathrm{FOM} = \mathrm{Re}(n)/\mathrm{Im}(n)$); experimental and numerical values of FOM are plotted in the bottom-right panel of Fig. 2a. For most frequency ranges, especially in the lower portion below the electric resonance, the FOM stays above 10, with a peak value exceeding 100.

Although the possibility of raising the refractive index has been experimentally demonstrated for single-layer metamaterials, further insights can be acquired with an investigation into three-dimensional

high-index metamaterials. In order to investigate the bulk properties, quasi-three-dimensional high-index metamaterials containing up to five layers were fabricated and tested. The measured complex refractive index and FOM are plotted in Fig. 2b, along with the corresponding numerically extracted parameters for this five-layer high-index metamaterial with small interlayer spacing ($d = 1.62\ \mu m$). From the THz-TDS measurements and subsequent parameter extraction, the highest index of refraction of 33.22 is obtained at a frequency of 0.851 THz. Interestingly, the refractive index does not fall sharply at higher frequencies, and shows an extremely broadband high refractive index with a full-width at half-maximum (FWHM) of 1.15 THz. Although all of the effective refractive indices are given here for normal incidence, we have found that the high-index metamaterials are quite robust to incidence angle variations. This robustness has its origin in the weak dependence of effective permeability on the direction of incident magnetizing field (Supplementary Information).

The presence of coupling between layers of quasi-three-dimensional metamaterials leads to substantial differences in the refractive index and the transmission spectra when compared to single-layer metamaterials[7,28]. To better understand the influence of the number of layers (N) on the optical characteristics, we analysed the band structure and plotted the dispersion relation (Fig. 3b). The thickness of the unit cell ($d = 12.2\ \mu m$) was intentionally increased relative to those of the samples designed for high refractive index so that the interlayer coupling and the changes in the corresponding transmission spectra could be clearly investigated. The band structure is indicative of the limiting case of perfectly periodic metamaterials in the z-direction. In conjunction with the effective parameter description, the bandgap between 0.833 and 1.734 THz corresponds to the negative effective permittivity regime. As clearly shown in Fig. 3a, the transmission corresponding to these bandgap frequencies is gradually lowered as the number of layers is increased, which is indicative of a progressive bandgap formation. In addition to this bandgap formation, transmission peaks appear in the spectra, which can be interpreted several ways[28,29]. From a homogeneous slab description, the metamaterial can be treated as a Fabry–Pérot etalon. The round trip phase delay should be a non-negative integer multiple of 2π and the transmission of the slab is maximized under the condition $f_p = pc/2nNd$, where f_p denotes the frequency of the transmission peak, p is a non-negative integer and c is the speed of light. From a microscopic point of view, the transmission peaks originate from the Bloch-like modes that are phase-matched to the Fabry–Pérot resonance of the metamaterial slab. For example, the single transmission peak observed in the double-layer metamaterial corresponds to the Bloch mode that has a normalized wavenumber of $1/2 \times \pi/d$. Generalized to the samples with larger numbers of layers (Fig. 3a), the transmitting modes correspond to the Bloch modes having a wavenumber of $p/N \times \pi/d$, where $p = 0,\ldots, N-1$.

The value of the refractive index is a sensitive function of the gap width for the proposed high-index metamaterials. Bearing this in mind, the question of the positive limit of a physically achievable refractive index naturally arises. To experimentally approach this limit, we measured the refractive index of metamaterials having gap widths from 80 nm to 30 μm. Figure 4a shows the measured and numerically estimated indices of refraction as a function of the gap width (top panel, peak index and the index at the quasi-static limit; bottom panel, peak index frequency). Theoretical refractive indices obtained from an empirical asymptotic formula are also plotted for the quasi-static limit (see Supplementary Information for the asymptotic formula and its limitations). The numerically estimated index is 26.6 at the quasi-static limit and increases to 54.87 at 0.315 THz for the sample with 80 nm gap width (the experimentally measured value was greater than 20 at the quasi-static limit and 38.64 at its peak; Fig 4b and c). In the weakly coupled regime, the capacitive coupling between unit cells is negligible so that the refractive index can be approximated as

$$n \approx n_p \left\{ 1 + \frac{\pi\alpha L}{2\sqrt{2}d}\left(1-\frac{g}{L}\right)^3 + \frac{\pi\alpha\beta L}{2\sqrt{2}d}\left(1-\frac{g}{L}\right)^4 \right\}$$

where α and β are dimensionless fitting parameters. However, as the gap width decreases, the capacitive effect due to coupling between unit cells becomes dominant. As a result, the index of refraction is drastically increased, with a dominant term proportional to the inverse $(1-\beta)/2$-th power of the gap width, $n \propto n_p \alpha^{1/2} d^{-1/2} L^{(2-\beta)/2} g^{-(1-\beta)/2}$, to the

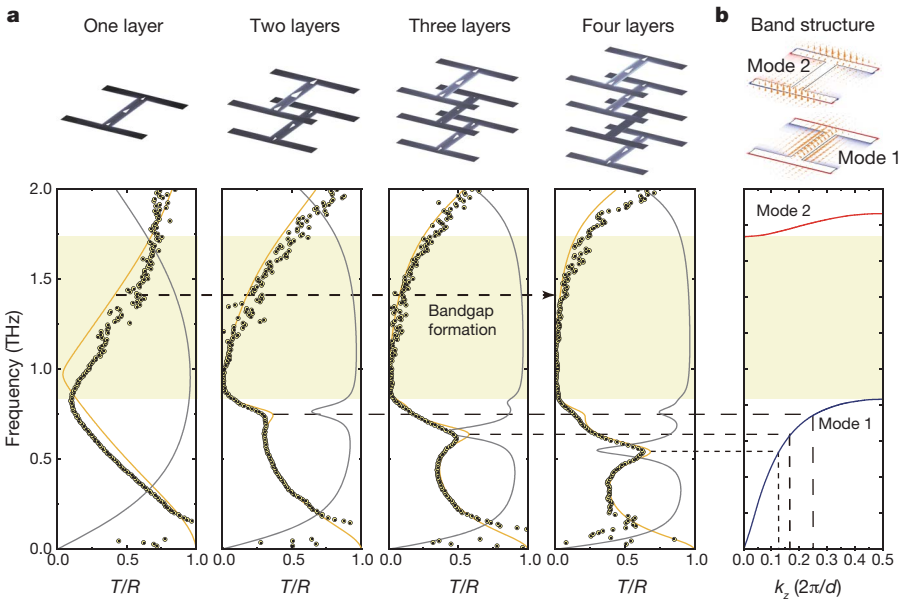

Figure 3 | Transmission/reflection spectra of multilayer metamaterials and the band structure. **a**, Main panels, transmission (T) and reflection (R) spectra for (left to right) single-, double-, triple- and quadruple-layer metamaterials. Here, the gap width g is set to 1.725 μm, the length of unit cell L is 40 μm, the width of the metallic structure w is 5 μm, and the thickness d of the unit cell is 12.2 μm for the simulations. In the transmission spectra measured for these multilayer metamaterials, shading corresponding to the bandgap frequencies (in Fig. 3b) is overlaid to show the progressive bandgap (rejection band) formation. Data points, experimental transmission; grey and orange lines, numerically calculated reflection and transmission, respectively. Top panels, the magnitude (colour map) and direction (arrow) of current density flowing in each layer for the corresponding metamaterial. **b**, Main panel, band structure calculated for the unit cell of the metamaterial. Top panel, corresponding electric (colour map) and magnetic field (arrow) profiles of band edge modes 1 and 2.

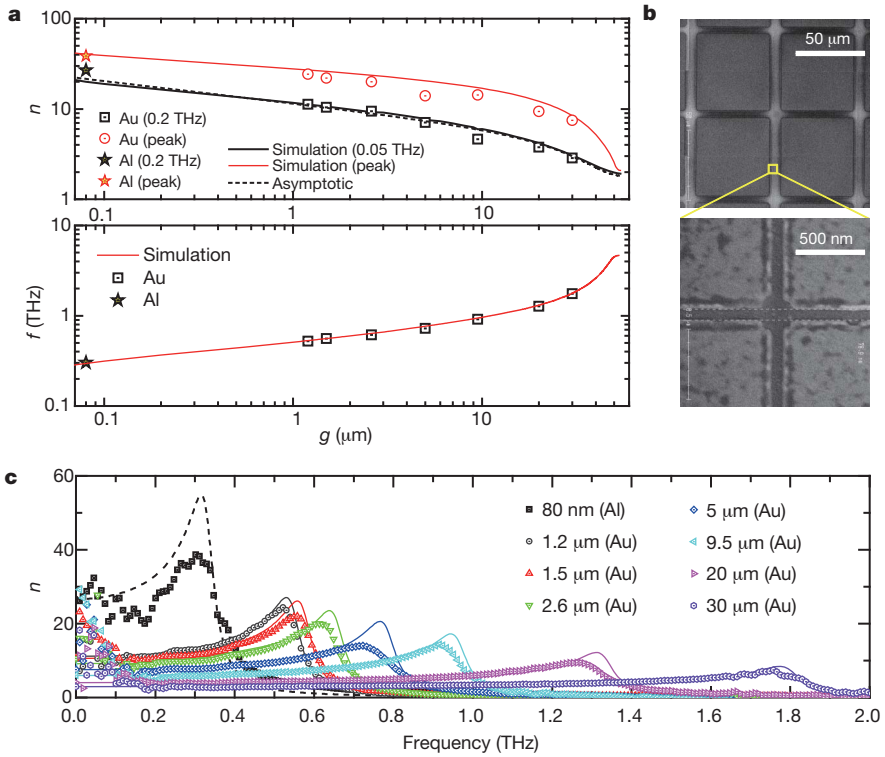

Figure 4 | Effective refractive index and peak index frequency as a function of the gap width for a single-layer metamaterial. **a**, Top, experimentally obtained refractive index n as a function of the gap width g. The quasi-static limits (near 0.2 THz) and the peak indices are plotted along with asymptotic and numerical values. Here, metamaterials are composed of a unit cell with $L = 60\,\mu m$, $d = 2.45\,\mu m$ and $w = 3\,\mu m$. Data points and lines show experimental and simulation data, respectively. Bottom, frequencies f of peak refractive index are plotted as a function of the gap width, along with simulated values. **b**, Scanning electron micrographs of a nanogap (~80 nm) high-index metamaterial ($d = 1.24\,\mu m$). The metal used to define the metallic patch is aluminium (Al) for this specific sample. **c**, Frequency dependent effective refractive indices of single-layer metamaterials with varying gap widths.

first order (provided that the gap width is larger than the metal thickness). Furthermore, once the gap width becomes smaller than the thickness of the metallic patch, the effective refractive index will increase even faster as the parallel plate capacitor regime is reached ($n \propto n_p(t/g)^{1/2}$, see Supplementary Information). Therefore, it should be possible to achieve an even higher index of refraction by further reducing the gap width (g) or the spacing (d) between each metamaterial layer. As the gap closes, this increase is expected to continue until the gap width approaches the Thomas–Fermi length scale[30] or the quantum tunnelling scale of electrons. In addition to this gap width control, it is worth noting that the effective refractive index is proportional to the substrate index; thus, the introduction of a higher-index substrate (such as lead sulphide or strontium titanate) will lead to greater amplification of the refractive index and an unprecedentedly large effective refractive index.

The artificial high-refractive-index material demonstrated here can extend the spectrum of indices further into the positive regime and broaden the realm of metamaterials having the previously demonstrated negative index[3–8], although we note that enhancement of the value of the negative index is still much in demand. In particular, high-index metamaterials, owing to the rapid phase advance associated with them, could be an ideal starting point for development of subwavelength-scale functional devices; such devices include small-footprint cloaking devices, wide-angle metamaterial lenses, compact cavity resonators and broadband slow light devices. The operating principles of high-index metamaterials are universal and can be extended to even lower frequency ranges, such as microwaves and radio frequencies, as well as to near-infrared or visible frequencies once the difficulties in fabrication have been resolved.

METHODS SUMMARY

Fabrication processes for micrometre-gap metamaterials. Fabrication of multilayered flexible terahertz metamaterials started with a bare silicon substrate as a sacrificial wafer. A polyimide solution (PI-2610, HD MicroSystems) was spin-coated onto the substrate and baked at 180 °C in a convection oven for 30 min as a flexible metamaterial substrate. The curing process of the polyimide layers was conducted at 350 °C using an open-ended quartz tube furnace under an inert atmosphere to convert the polyamic acid into a fully aromatic and insoluble polyimide. A negative photoresist (AZnLOF2035, AZ Electronic Materials) was spin-coated and patterned using conventional photolithography. Au/Cr (90 nm/10 nm) was then evaporated and patterned as 'I'-shaped array structures via the lift-off technique. Repeating the polyimide coating and curing processes, single-layered metamaterials were fabricated. Multilayered metamaterials on the silicon substrate were obtained by repeating the above single-layer processes until the desired number of metamaterial layers was stacked. Finally, the flexible terahertz metamaterials were fabricated by peeling off the metamaterial layers from the silicon substrate. The dimensions of the micrometre-gap metamaterials were estimated by optical microscopy, stylus profiler, and 3D profiler.

Fabrication processes for nano-gap metamaterial. Nano-gap flexible terahertz metamaterials were fabricated using the same process for the micrometre-gap metamaterials except for the nano-gap patterning process, which used electron beam lithography and consecutive metal etching. Thin aluminium film was evaporated onto the polyimide coated silicon substrate and patterned as a connected 'I'-shaped patch structure using the lift-off technique. Etching windows for 80-nm gaps were opened using large area electron beam lithography. An 'I'-shaped aluminium beam array was patterned by RIE (reactive ion etching) using an electron beam resist mask (ZEP520A, ZEON Corporation). After removing the residual resist and after the polyimide coating process, the nano-gap terahertz metamaterials were fabricated on the silicon sacrificial substrate.

Full Methods and any associated references are available in the online version of the paper at www.nature.com/nature.

Received 25 August; accepted 13 December 2010.

1. Veselago, V. G. The electrodynamics of substances with simultaneously negative values of ε and μ. *Sov. Phys. Usp.* **10,** 509–514 (1968).
2. Pendry, J. B., Holden, A. J., Robbins, D. J. & Stewart, W. J. Magnetism from conductors and enhanced nonlinear phenomena. *IEEE Trans. Microwave Theory Tech.* **47,** 2075–2084 (1999).

3. Smith, D. R., Padilla, J. W., Vier, D. C., Nemat-Nasser, S. C. & Schultz, S. Composite medium with simultaneously negative permeability and permittivity. *Phys. Rev. Lett.* **84,** 4184–4187 (2000).
4. Shelby, R. A., Smith, D. R. & Schultz, S. Experimental verification of a negative index of refraction. *Science* **292,** 77–79 (2001).
5. Eleftheriades, G. V., Iyer, A. K. & Kremer, P. C. Planar negative refractive index media using periodically L–C loaded transmission lines. *IEEE Trans. Microwave Theory Tech.* **50,** 2702–2712 (2002).
6. Xiao, S. *et al.* Loss-free and active optical negative-index metamaterials. *Nature* **466,** 735–738 (2010).
7. Valentine, J. *et al.* Three-dimensional optical metamaterial with a negative refractive index. *Nature* **455,** 376–379 (2008).
8. Zhang, S. *et al.* Negative refractive index in chiral metamaterials. *Phys. Rev. Lett.* **102,** 023901 (2009).
9. Pendry, J. B., Schrurig, D. E. & Smith, D. R. Controlling electromagnetic fields. *Science* **312,** 1780–1782 (2006).
10. Schurig, D. *et al.* Metamaterial electromagnetic cloak at microwave frequencies. *Science* **314,** 977–980 (2006).
11. Cai, W. S., Chettiar, U. K., Kildishev, A. V. & Shalaev, V. M. Optical cloaking with metamaterials. *Nature Photon.* **1,** 224–227 (2007).
12. Liu, R. *et al.* Broadband ground-plane cloak. *Science* **323,** 366–369 (2009).
13. Valentine, J., Li, J. S., Zentgraf, T., Bartal, G. & Zhang, X. An optical cloak made of dielectrics. *Nature Mater.* **8,** 568–571 (2009).
14. Gabrielli, L. H., Cardenas, J., Poitras, C. B. & Lipson, M. Silicon nanostructure cloak operating at optical frequencies. *Nature Photon.* **3,** 461–463 (2009).
15. Pendry, J. B. Negative refraction makes a perfect lens. *Phys. Rev. Lett.* **85,** 3966–3969 (2000).
16. Liu, Z., Lee, H., Xiong, Y., Sun, C. & Zhang, X. Far-field optical hyperlens magnifying sub-diffraction-limited objects. *Science* **315,** 1686 (2007).
17. Smolyaninov, I. I., Hung, Y. J. & Davis, C. C. Magnifying superlens in the visible frequency range. *Science* **315,** 1699–1701 (2007).
18. Palik, E. D. *Handbook of Optical Constants of Solids* (Academic, 1998).
19. Enkrich, C. *et al.* Magnetic metamaterials at telecommunication and visible frequencies. *Phys. Rev. Lett.* **95,** 203901 (2005).
20. Sievenpiper, D. F. *et al.* 3D metallo-dielectric photonic crystals with strong capacitive coupling between metallic islands. *Phys. Rev. Lett.* **80,** 2829–2832 (1998).
21. Shen, J. T., Catrysse, P. B. & Fan, S. Mechanism for designing metallic metamaterials with a high index of refraction. *Phys. Rev. Lett.* **94,** 197401 (2005).
22. Shin, J., Shen, J. T. & Fan, S. Three-dimensional metamaterials with an ultrahigh effective refractive index over a broad bandwidth. *Phys. Rev. Lett.* **102,** 093903 (2009).
23. Smith, D. R., Vier, D. C., Koschny, Th & Soukoulis, C. M. Electromagnetic parameter retrieval from inhomogeneous metamaterials. *Phys. Rev. E* **71,** 036617 (2005).
24. Tao, H. *et al.* Terahertz metamaterials on free-standing highly-flexible polyimide substrates. *J. Phys. D Appl. Phys.* **41,** 232004 (2008).
25. Liu, R., Cui, T. J., Huang, D., Zhao, B. & Smith, D. R. Description and explanation of electromagnetic behaviors in artificial metamaterials based on effective medium theory. *Phys. Rev. E* **76,** 026606 (2007).
26. Ferguson, B. & Zhang, X. C. Materials for terahertz science and technology. *Nature Mater.* **1,** 26–33 (2002).
27. Duvillaret, L., Garet, F. & Coutaz, J. L. A reliable method for extraction of material parameters in terahertz time-domain spectroscopy. *IEEE J. Sel. Top. Quantum Electron.* **2,** 739–746 (1996).
28. Liu, N. & Giessen, H. Three-dimensional optical metamaterials as model systems for longitudinal and transverse magnetic coupling. *Opt. Express* **16,** 21233–21238 (2008).
29. Papasimakis, N. *et al.* Metamaterial analog of electromagnetically induced transparency. *Phys. Rev. Lett.* **101,** 253903 (2008).
30. Seo, M. A. *et al.* Terahertz field enhancement by a metallic nano slit operating beyond the skin-depth limit. *Nature Photon.* **3,** 152–156 (2009).

Supplementary Information is linked to the online version of the paper at www.nature.com/nature.

Acknowledgements We thank B. Kang for help in the fabrication of micrometre-gap metamaterials, J. S. Chang for proofreading the manuscript before submission, and D. S. Kim for discussions. This work was supported by National Research Foundation of Korea grants funded by the Korean government (numbers 2009-0069459, 2008-0062235 and 2010-0012058). K.-Y.K. acknowledges support by the IT Research and Development programme of MKE/KEIT (number 2006-S-005-04). Y.-H.L. acknowledges support from the National Research Foundation of Korea (number 2007-0093863) and N.P. acknowledges support from National Research Foundation (numbers GRL K20815000003 and 2010-0001859), funded by the Korean government.

Author Contributions M.C. and Y.K. performed the numerical simulations. S.H.L. fabricated micro/nano-gap metamaterial samples. S.B.K., M.H.K. and K.-Y.K. conducted THz-TDs experiments. M.C., S.H.L., Y.K., J.S. and B.M. analysed numerical and experimental data. M.C., S.H.L., Y.K., J.S., Y.-H.L., N.P. and B.M. discussed the results. M.C., J.S., Y.-H.L., N.P. and B.M. wrote the manuscript. B.M. led the overall direction of the project.

Author Information Reprints and permissions information is available at www.nature.com/reprints. The authors declare no competing financial interests. Readers are welcome to comment on the online version of this article at www.nature.com/nature. Correspondence and requests for materials should be addressed to B.M. (bmin@kaist.ac.kr).

METHODS

THz-TDS measurement. A conventional transmission-type THz-TDS system was used for the characterization of the fabricated metamaterials. A key component for generating and detecting the THz pulse is a photoconductive dipole antenna irradiated with femtosecond laser pulses (30–50 fs) from a Ti:sapphire laser with a repetition rate of 80 MHz. We used a dipole antenna fabricated on a low-temperature-grown GaAs (LT-GaAs) film with 5 μm gap and 30 μm length. The emitter antenna is d.c. biased from 10 V to 20 V and generates terahertz pulses with most of the spectral power density between 0.2 THz and 3 THz. The receiving antenna was fabricated on an LT-GaAs film and consisted of a coplanar transmission line structure with a 5 μm gap and 30 μm length. The metamaterial samples were attached to a sample holder that has an optical aperture 15 mm in diameter. An identical clear aperture was used as a free-space transmission reference. When the thickness of the samples is large enough, the first transmitted terahertz pulse and the following echoes caused by internal Fabry–Pérot reflection are temporally well separated. However, for the fabricated high-index metamaterials, the thickness was relatively small and the resulting transmitted pulse was the superposition of the components from multiple internal Fabry–Pérot reflections. Therefore, in order to reliably extract the effective parameters (complex refractive index), a numerical iterative method was used to minimize errors in the phase and magnitude.

Effective thickness estimation. Assignment of effective indices to a single-layer metamaterial must be made with extreme care, especially when there are no explicit physical boundaries (though this is not the case for the present work). Based on the criterion that the effective thickness should be defined as a distance between virtual boundaries, at which the reflected and transmitted wave behave like plane waves[31] (this condition is equivalent to considering the decay length of the mode), we conducted additional simulations with increasing numbers of metamaterial layers and compared their effective refractive indices and the impedance at the quasi-static limit with that of a single-layer metamaterial. As the number of metamaterial layers increases, the effect of mode decay at the ends of the metamaterial becomes negligible; accordingly, the bulk refractive index can be defined as the converging value. As the effective refractive index (especially at the quasi-static limit) should be invariant with respect to the number of metamaterial layers, the effective thickness of a single-layer metamaterial can be defined as the thickness that renders the same bulk refractive index at the quasi-static limit. For example (corresponding to Fig. 2a), without the scaling, the refractive index at the quasi-static limit differ from the bulk value by ~12%. Therefore, the refractive index (at the quasi-static limit) of the single-layer metamaterial decreases from 11.1 to 9.72 with an effective thickness of 2.79 μm (note that the physical thickness is 2.45 μm for this sample).

31. Chen, X., Grzegorczyk, T. M., Wu, B.-I., Pacheco, J. & Kong, J. A. Robust method to retrieve the constitutive effective parameters of metamaterials. *Phys. Rev. E* **70,** 016608 (2004).